Near-Infrared Photoluminescence Enhancement in Ge/CdS and Ge/ZnS Core/Shell Nanocrystals: Utilizing IV/II–VI Semiconductor Epitaxy

Yijun Guo,[†,‡] Clare E. Rowland,[§,⊥] Richard D. Schaller,[§,⊥] and Javier Vela[†,‡,*]

[†]Department of Chemistry, Iowa State University, Ames, Iowa 50010, United States, [‡]Ames Laboratory, Ames, Iowa 50011, United States, [§]Center for Nanoscale Materials, Argonne National Laboratory, Argonne, Illinois 60439, United States, and [⊥]Department of Chemistry, Northwestern University, Evanston, Illinois 60208, United States

ABSTRACT Ge nanocrystals have a large Bohr radius and a small, size-tunable band gap that may engender direct character *via* strain or doping. Colloidal Ge nanocrystals are particularly interesting in the development of near-infrared materials for applications in bioimaging, telecommunications and energy conversion. Epitaxial growth of a passivating shell is a common strategy employed in the synthesis of highly luminescent II–VI, III–V and IV–VI semiconductor quantum dots. Here, we use relatively unexplored IV/II–VI epitaxy as a way to enhance the photoluminescence and improve the optical stability of colloidal Ge nanocrystals. Selected on the basis of their relatively small lattice mismatch compared with crystalline Ge, we explore the growth of epitaxial CdS and ZnS shells using the successive ion layer adsorption and reaction method. Powder X-ray diffraction and electron microscopy techniques, including energy dispersive X-ray spectroscopy and selected area electron diffraction, clearly show the controllable growth of as many as 20 epitaxial monolayers of CdS atop Ge cores. In contrast, Ge etching and/or replacement by ZnS result in relatively small Ge/ZnS nanocrystals. The presence of an epitaxial II–VI shell greatly enhances the near-infrared photoluminescence and improves the photoluminescence stability of Ge. Ge/II–VI nanocrystals are reproducibly 1–3 orders of magnitude brighter than the brightest Ge cores. Ge/4.9CdS core/shells show the highest photoluminescence quantum yield and longest radiative recombination lifetime. Thiol ligand exchange easily results in near-infrared active, water-soluble Ge/II–VI nanocrystals. We expect this synthetic IV/II–VI epitaxial approach will lead to further studies into the optoelectronic behavior and practical applications of Si and Ge-based nanomaterials.

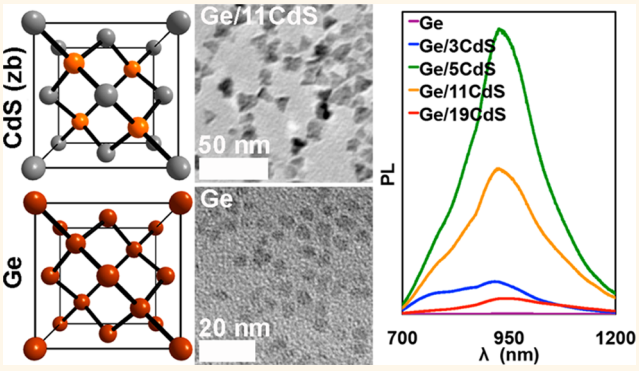

KEYWORDS: germanium · core/shell nanocrystals · IV/II–VI epitaxy · near-IR photoluminescence · quantum dots

Elemental germanium (Ge) is a relatively abundant and robust covalent semiconductor.[1] Ge has a small indirect band gap (0.661 eV or 1876 nm) and a large Bohr radius (24 nm), which together theoretically provide for a wide range of emission energies attainable *via* size-tunable quantum confinement.[2–4] Further, recent reports suggest that strain[5–7] and doping strategies[8] may result in direct band gap Ge nanostructures. As such, Ge is particularly interesting in the development of near-infrared (near-IR) active quantum dot fluorophores for applications in biology (imaging and tracking), telecommunications, and energy conversion (photovoltaics, photocatalysis).

Different routes exist for the synthesis of low dimensional Ge. Reduction of GeI_2 with $LiAlH_4$[9] or hexamethyldisilazane/oleylamine[10] and microwave reduction of GeI_2 and GeI_4 with oleylamine result in colloidal Ge nanocrystals.[11] Reduction of $Ge(OEt)_4$ with trialkoxysilanes[12] and thermal processing of polymeric sol–gel organogermanium oxides $(-PhGeO_{1.5}-)$[13,14] result in SiO_2- and GeO_2-supported Ge nanocrystals, respectively. Pulsed-laser photolysis of $GeMe_4$ in the gas phase also yields Ge nanocrystals.[15] Thermal disproportionation of hydrogen silsesquioxane ($H_8Si_8O_{12}$) and GeI_2 results in $Si_{0.45}Ge_{0.55}$ nanocrystals.[16] A mixed valence iodide reduction method enables the

* Address correspondence to vela@iastate.edu.

Received for review May 22, 2014 and accepted July 10, 2014.

Published online July 10, 2014
10.1021/nn502792m

synthesis of alloyed $Ge_{1-x}E_x$ nanocrystals (E = Al, P, Ga, As, In, Sn, Sb; $x \approx 1\%$) with high incorporation efficiency (45−100%).[17]

Some Ge syntheses reportedly produce fluorescent (photoluminescent) Ge nanocrystals. Reduction of $GeCl_4$ with $NaBH_4$ in polyvinylpyrrolidone (PVP) at room temperature (rt)[18] and laser ablation of H-terminated Ge wafers[19] produce violet (380 nm) and blue (450 nm) emitting Ge nanocrystals, respectively. Templated oxidative polymerization of Zintl $(Ge_9)^{4-}$ clusters produces hexagonal Ge mesopores (3.1−3.2 nm pore size) characterized by large surface areas (404−451 m^2/g) and tunable (1.3−2.2 nm), wall thickness-dependent photoluminescence (PL, 640−672 nm).[20−25] A small subset of available syntheses are believed to produce Ge nanocrystals that emit in the near-IR (800−2500 nm, also called "NIR" region). Reduction of GeI_2 with nBuLi in hexadecylamine,[26] GeI_4 and GeI_2 with hexadecyl- or oleyl-amine,[27] or gaseous $GeCl_4$ with H_2 in a plasma were reported to produce near-IR emitting Ge nanocrystals with tunable band gap.[28] Although near-IR PL quantum yields as high as 8% were originally reported,[26] these are now know believed to be much lower, and typically hover between zero (0) and below 1%. Epitaxial growth of a surface-passivating layer is a common strategy employed in the synthesis of highly luminescent II−VI, III−V and IV−VI semiconductor quantum dots.[29−38] Here, we utilize relatively unexplored IV/II−VI epitaxy to enhance the photoluminescence and improve the optical stability of Ge nanocrystals.[39,40]

RESULTS AND DISCUSSION

Ge Crystal Chemistry. Elemental germanium adopts the diamond crystal structure that is common to all group IV semiconductors (C, Si, Ge, Sn, Pb) (Figure 1). This diamond structure is topologically similar to, or isotopic with the zinc blende (sphalerite) crystal structure adopted by many II−VI and III−V semiconductors. In both the diamond and zinc blende structures, each and every atom (or ion) is tetrahedrally coordinated. In the diamond structure, the same atom occupies all positions (for example, Ge as in Ge−Ge−Ge−Ge) (Figure 1a), whereas in the zinc blende structure, two different ions alternate positions (for example, Zn^{2+} and S^{2-} as in Zn−S−Zn−S) (Figure 1b).

Selecting Shell Materials for Ge Epitaxy. Because highly crystalline semiconductors tend to possess superior optical qualities, core/shell and multilayer nanostructures require the structure of their individual components to be similar enough so that all interfacial boundaries remain defect-free. In other words, interfacial epitaxy between the different phases must have strict continuity. In a core/shell, this can only be accomplished when the core and shell materials have identical and/or very similar crystal structures or, more specifically, when both materials are isostructural (isotopic) and share a similar lattice constant

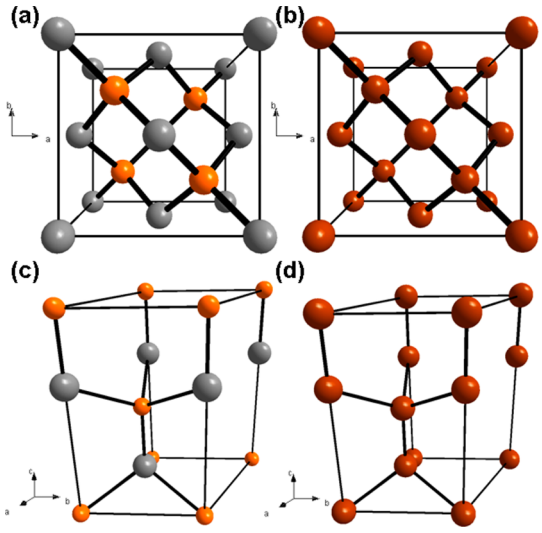

Figure 1. Unit cells of (a) cubic ZnS or CdS (zinc blende), (b) cubic Ge (diamond), (c) hexagonal ZnS or CdS (wurtzite), and (d) hypothetical hexagonal Ge (gray: Zn or Cd; orange: S; brown: Ge).

(exceptions are uncommon among optical materials[41,42]). As an example, the small lattice mismatch (−3.7%, Table 1) between isostructural CdSe and CdS allowed the growth of thick epitaxial CdS shells on top of CdSe cores.[43−45] The resulting high quality, "giant" CdSe/CdS core/shell nanocrystals remain the best example of nonblinking quantum dot fluorophores to date,[46−52] which allowed their use in 3D superlocalization, dynamic tracking, and subdiffraction spatial resolution luminescence depletion imaging.[53−55] In contrast, the large lattice mismatch (−11%, Table 1) between CdSe and ZnS did not allow the growth of real (complete) ZnS shells on CdSe cores. Only isolated ZnS islands could be grown on the surface of CdSe cores.[56] For this reason, we decided to investigate shell materials that can adopt a cubic, zinc blende structure with a similar lattice parameter to that of cubic, diamond Ge. Several II−VI and III−V semiconductors are available for this purpose (Table 1). However, we focused on II−VI semiconductors because these are known to be much more chemically and photochemically robust compared to III−V semiconductors. Here, we specifically explore CdS and ZnS as shell materials because the lattice mismatch between these and Ge is relatively small at +3.1 and −4.4, respectively (Table 1). In addition, the valence and conduction energy levels of Ge, CdS and ZnS are such that either type I (Ge/ZnS, Ge/CdS) or quasi-type II (Ge/CdS) heterostructures could be possible depending on the relative size of the Ge core and the thickness of the II−VI shell (Figure 2).[47]

IV/II−VI Epitaxy: Synthesis of Ge/CdS Core/Shell Nanocrystals. Nanocrystalline Ge cores, freshly synthesized by reduction of GeI_2 with *n*-butyllithium,[32] were reacted with enough Cd and S precursors alternately to form one atomic monolayer (ML) of CdS at a time using the successive ion layer adsorption and reaction (SILAR) method.[44,57] We originally carried out this procedure

TABLE 1. Structural and Optical Properties of II–VI and IV Semiconductors: Cores *vs* Possible Epitaxial Shell Materials

core/shell	crystal structure	lattice parameters, Å (% lattice mismatch)[c]	band gap type	bulk value, eV (nm)	core quantized (qdot) range, eV (nm)
IV/IV and IV/II–VI core/shells					
Ge/	diamond	5.658 (0)	indirect	0.664 (1870)	1.46–0.77 (850–1600)
Si	diamond	5.431 (−4.0)	indirect	1.12 (1110)	–
CdS	zinc blende	5.832 (+3.1)	direct	2.40 (520)	–
ZnS	zinc blende	5.4063 (−4.4)	direct	3.60 (344)	–
ZnSe	zinc blende	5.6676 (+0.17)	direct	2.70 (460)	–
II–VI/II–VI core/shells (previously synthesized[29,30,43–45])					
CdSe/	wurtzite[a]	4.299, 7.010 (0)	direct	1.74 (713)	2.53–1.94 (490–640)
CdS	wurtzite[a]	4.1348, 6.749 (−3.7)	direct	2.40 (520)	–
ZnS	wurtzite[a]	3.814, 6.258 (−11)	direct	3.60 (344)	–
III–V/II–VI core/shells (previously synthesized[31,36–38])					
InP/	zinc blende[a]	5.86875 (0)	direct	1.34 (925)	2.53–1.77 (490–700)
CdS	zinc blende[a,b]	5.832 (−0.63)	direct	2.40 (520)	–

[a] Calculated lattice mismatches for II–VI/II–VI and III–V/II–VI core/shells are similar regardless of whether zinc blende (cubic) or wurtzite (hexagonal) structures are considered. [b] InP/CdS were reported to have a wurtzite structure. [c] Calculated as 100 × [(shell lattice parameter − core lattice parameter)/core parameter]; positive (+) and negative (−) values correspond to core-to-shell lattice expansion and compression, respectively.

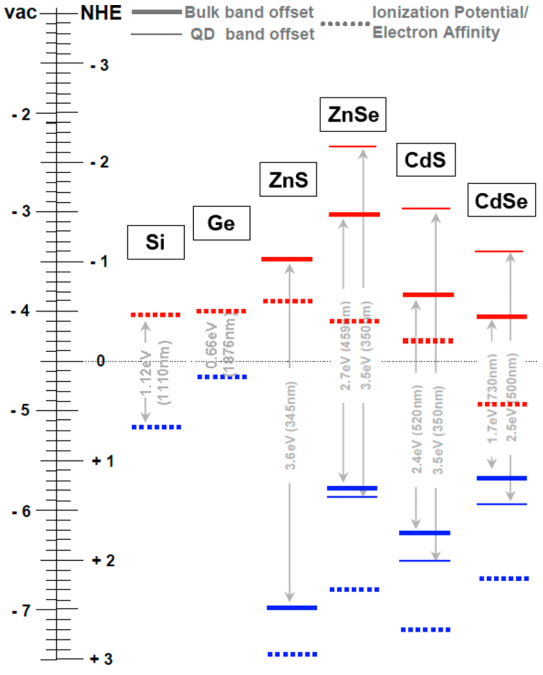

Figure 2. Compilation of valence and conduction energy levels, as well as ionization potentials and electron affinities reported for Ge, ZnS and CdS semiconductors. Si, ZnSe and CdSe are also shown for comparison. The "QD" levels represent maximum band gap widening due to the effect of quantum confinement in low dimensional (nanosized) semiconductors.

by adding the S precursor solution first, followed by adding the Cd precursor solution (S first, Cd second). On the basis of the relative electronegativity values ($\chi_{Pauling}$) of Ge (2.01), S (2.58) and O (3.44), oxidation of Ge by S is similar to its oxidation by oxygen, but with a smaller driving force. We thus speculated this could permit a mild and controllable, shallow oxidation of the outermost layer of Ge atoms by S, forming strong Ge–S bonds and allowing shell growth to initiate more smoothly (Scheme 1). However, subsequent experiments showed that the specific order of precursor addition does not matter. Starting with Cd precursor addition, followed by S addition (Cd first, S second) was just as effective in growing thick CdS shells atop Ge cores.

Figure 3 shows transmission electron microscopy (TEM) analyses for a typical shell growth procedure. Starting with cubic Ge cores (with a size or diameter of 4.6 ± 0.7 nm), we were able to grow Ge/*n*CdS with varying shell thicknesses of up to *ca.* n = 20 CdS monolayers (MLs): Ge/3.1CdS (6.4 ± 0.8 nm), Ge/4.9CdS (7.4 ± 1.0 nm), Ge/10.5CdS (10.7 ± 1.3 nm), and Ge/18.8CdS (15.5 ± 1.8 nm) (Table 2). All the Ge/CdS core/shell nanocrystal samples have a narrow size distribution (11–13%), comparable or narrower than the initial Ge cores (15%); thus, their isolation did not require any size selection.

During CdS shell growth, the shape of the Ge/CdS core/shells slowly transforms from spheres (Ge and Ge/3.1CdS) to tetrahedral prisms (Ge/10.5CdS and Ge/18.8CdS) (Figure 3a–d). A tetrahedral morphology is usually a strong indication of a cubic crystal structure. However, powder X-ray diffraction (XRD) (Figure 4) and selected area electron diffraction (SAED) (Figure 3f) are both consistent with all the Ge/CdS core/shells containing a mixture of hexagonal and cubic structures. We believe a plausible explanation for the observed shape evolution is that the original cubic (diamond) structure of the Ge cores could be dictating the final shape of the Ge/CdS core/shells. Crystalline Ge is a covalent material made up of strong Ge–Ge bonds. Cubic to hexagonal transformations of Ge may thus involve a large activation energy barrier and may not be nearly as common as for II–VI semiconductors. In fact, hexagonal Ge remains unknown under standard ambient conditions. In contrast, the epitaxial CdS shell could easily adopt a hexagonal (wurtzite) structure, or a cubic (zinc blende) structure, or any combination of the two. On the basis of the XRD data, Ge/*n*CdS core/shells

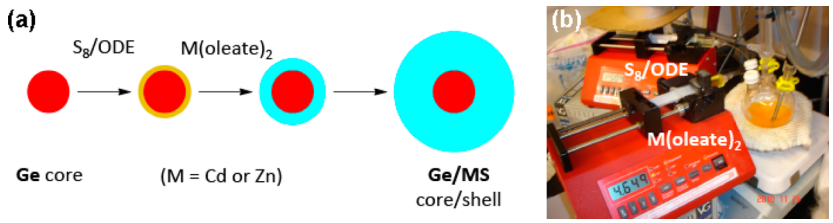

Scheme 1. Illustration of the sulfur-based surface "priming" approach initially used in the synthesis of Ge/CdS and Ge/ZnS core/shell nanocrystals (a). The experimental setup uses two programmable syringe pumps containing the two separate M (Cd or Zn) and S precursor solutions (b).

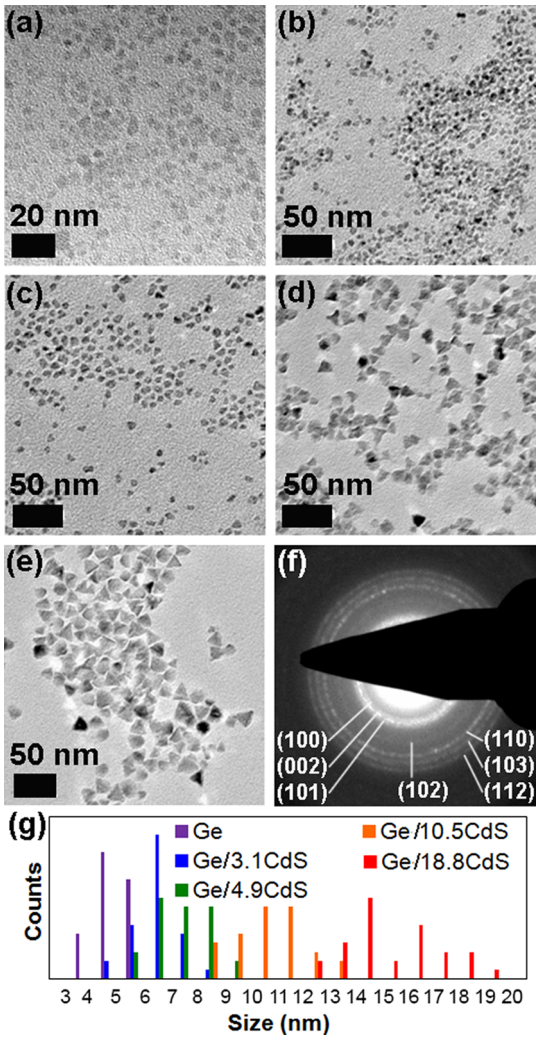

Figure 3. Ge core and thick-shell Ge/*n*CdS core/shell nanocrystals (*n* = number of MLs): (a) Ge (4.6 ± 0.7 nm), (b) Ge/3.1CdS (6.4 ± 0.8 nm), (c) Ge/4.9CdS (7.4 ± 1.0 nm), (d) Ge/10.5CdS (10.7 ± 1.3 nm), (e) Ge/18.8CdS (15.5 ± 1.8 nm), (f) SAED pattern of Ge/4.9CdS nanocrystals, and (g) overall size histograms (>200 particles counted in each case).

having between 5 and 19 MLs are anywhere between 7 and 17% cubic and between 83 and 93% hexagonal (see Methods). This is consistent with the fraction of the core/shells made up by the relatively small Ge core. On the basis of the number of MLs calculated from TEM data (size histograms), the theoretical Ge core volume falls quickly from 23 to 3% on going from Ge/4.9CdS to Ge/18.8CdS, respectively (Table 2). We also note that, among the possible impurities for Ge-based materials, neither the initial Ge cores nor the resulting Ge/CdS core/shells showed any conclusive evidence of GeO_2, GeS_2 or GeS (Figure 4).

Elemental mapping and composition analyses of several individual particles by energy dispersive X-ray spectroscopy (EDX) confirmed the presence and homogeneous distribution of all three Ge, Cd and S elements within all particles. These data, summarized in Table 2, show good agreement with the theoretical elemental composition calculated from the number of MLs obtained from TEM. Figure 5 shows representative EDX elemental mapping data for Ge/10.5CdS core/shell nanocrystals. Because the core makes only a very small fraction of the sample (*ca.* 8% in volume, see Table 2), the Ge signal-to-noise (S/N) ratio is low. Nevertheless, we found no evidence of phase segregation in any Ge/II–VI sample using EDX.

Synthesis of Ge/ZnS Nanocrystals. We explored a similar SILAR procedure to grow epitaxial ZnS shells on Ge cores. This resulted in Ge/ZnS nanocrystals (3.8 ± 0.7 nm) that are of comparable size or even slightly smaller than the initial Ge cores (4.6 ± 0.7 nm) (see Figure S1, Supporting Information, and Table 2). EDX data of several such particles across multiple areas of different samples consistently showed the presence of all three Ge, Zn and S in significant ratios: 13 ± 3, 37 ± 5 and 49 ± 5 atom %, respectively (Table 2). Of course, it is impossible for the particle size to decrease upon shell growth. Thus, the original Ge cores must be undergoing either etching and/or partial exchange by ZnS.[33,34,58–61] Because the resulting nanocrystals still show the NIR photoluminescence characteristic of Ge, these nanocrystals must have either a core/shell or graded Ge/ZnS composition.[62] Why this etching or exchange occurs with ZnS and not with CdS is presently unknown, but there are some clues: On the basis of lattice parameters, ZnS leads to compression (−4.4%) while CdS leads to expansion (+3.1%) of the Ge core (Table 1). In addition, according to Pearson's theory of hard and soft acids and bases (HSAB),[63,64] Zn^{2+} is a borderline acid while Cd^{2+} is a soft acid. Also, the 0.1 M Zn(oleate)$_2$ precursor solution contains a somewhat higher concentration of excess oleic acid (0.68 M) compared to the 0.1 M Cd(oleate)$_2$ precursor

TABLE 2. Synthesis of Ge/II–VI Core/Shell Nanocrystals

		composition: Ge, M (Cd or Zn), S			
sample	size (nm)	theoretical	EDS	theoretical Ge core volume[a] (%)	XRD phase(s)
Ge	4.6 ± 0.7	100, 0, 0	100, 0, 0	100	diamond (cubic)
Ge/3.1CdS	6.4 ± 0.8	40, 30, 30	16 ± 4, 43 ± 3, 41 ± 2	38	n.d.[c]
Ge/4.9CdS	7.4 ± 1.0	25, 38, 38	5 ± 2, 42 ± 6, 53 ± 7	23	17% zinc blende (cubic) + 83% wurtzite (hexagonal)
Ge/10.5CdS	10.7 ± 1.3	9, 46, 46	2.0 ± 0.5, 49 ± 4, 49 ± 4	8	7% zinc blende (cubic) + 93% wurtzite (hexagonal)
Ge/18.8CdS	15.5 ± 1.8	3, 49, 49	2 ± 1, 47 ± 6, 50 ± 6	3	12% zinc blende (cubic) + 88% wurtzite (hexagonal)
Ge/ZnS[b]	3.8 ± 0.7	n.d.[b]	13 ± 3, 37 ± 5, 49 ± 5	n.d.[c]	zinc blende (cubic)

[a] Theoretical Ge and II–VI volumes were calculated using the Ge core and II–VI shell sizes (diameters and thicknesses, respectively) measured by TEM. [b] Partial Ge etching may have occurred (see Supporting Information); exact no. of MLs unknown. [c] Not determined.

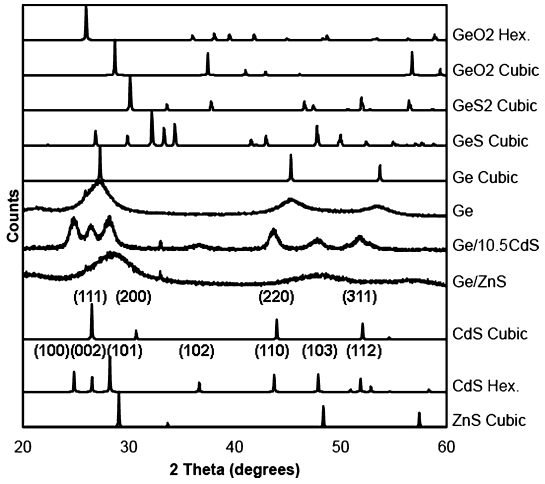

Figure 4. Powder X-ray diffraction patterns of Ge, Ge/CdS and Ge/ZnS nanocrystals (experimental), and of bulk GeO_2, Ge, CdS and ZnS (for comparison).

TABLE 3. Representative Photoluminescence Properties of Ge/II–VI Core/shell Nanocrystals

sample	QY (%)[a]	PL enhancement[b]	lifetime (ns)
Ge	0.0004	×1[b]	n.d.[c]
Ge/3.1CdS	0.050	×120	2280 ± 30
Ge/4.9CdS	1.2	×2930	2740 ± 11
Ge/4.9CdS in water	0.0029	×7	596 ± 52
Ge/10.5CdS	0.066	×160	2440 ± 32
Ge/18.8CdS	0.0060	×15	1820 ± 261
Ge/ZnS	0.23	×560	551 ± 13
Ge/ZnS in water	0.0072	×18	943 ± 19

[a] Typical error in QY determination is 15% of the indicated value (see Methods). [b] Relative PL intensity of the brightest Ge cores was arbitrarily set to 1. [c] Not determined: PL was too weak to accurately measure a lifetime.

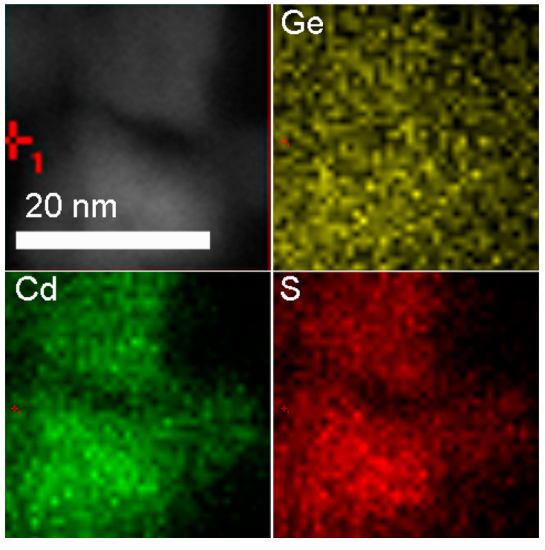

Figure 5. EDX elemental mapping of Ge/10.5CdS nanocrystals does not show any clear evidence of phase segregation (Notes: Shown are four identical or "registered" areas within the same sample; only 8% of this sample's volume is made of Ge, see Table 2).

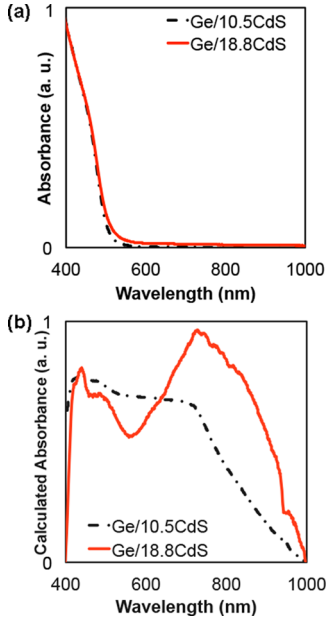

Figure 6. Representative solution phase absorption spectra (a) and solid phase (film) absorption spectra (calculated from diffuse reflectance data (b) for Ge/CdS core/shell nanocrystals. The two clear absorption edges evident at 520 nm (a) and *ca.* 800 nm (b) originate from the thick CdS shell[29,30,44,45] and Ge core,[26–28] respectively.

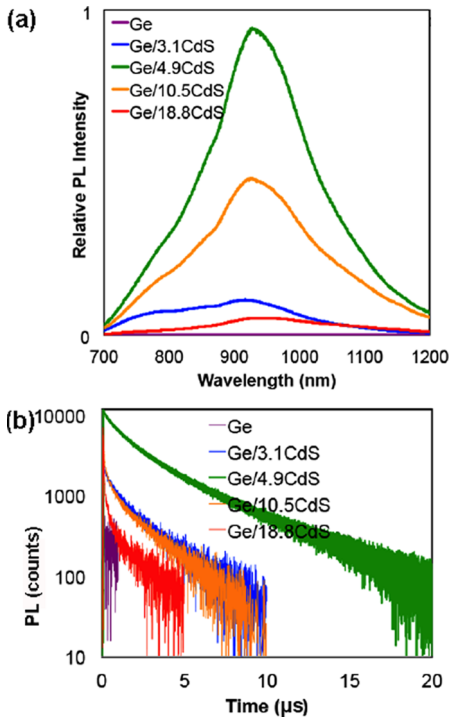

Figure 7. (a) Photoluminescence spectra of Ge, Ge/3.1CdS, Ge/4.9CdS, Ge/10.5CdS and Ge/18.8CdS nanocrystals (normalized by optical density (absorbance) at the excitation wavelength, λ_{exc} = 532 nm). (b) Time-resolved photoluminescence decay of Ge, Ge/3.1CdS, Ge/4.9CdS, Ge/10.5CdS and Ge/18.8CdS nanocrystals (λ_{exc} = 450 nm).

solution (0.24 M) (see Methods). Successful growth of thicker epitaxial ZnS shells on Ge cores will require further optimization of reaction conditions, and will be the subject of a separate article in the future.

Photoluminescence Enhancement in Ge/II–VI Nanocrystals. Growth of an epitaxial II–VI shell greatly enhances the NIR PL intensity and improves the NIR PL stability of Ge nanocrystals (Table 3, Figures 6 and 7). All the Ge/CdS core/shells and Ge/ZnS nanocrystals we have made showed NIR PL and retained their NIR PL over a period of several months, regardless of shell thickness or composition. Among the Ge/CdS core/shell nanocrystals with different number of MLs that we studied, Ge/4.9CdS had the highest NIR PL quantum yield of 1.2% (almost three thousand times brighter than the best Ge cores), as well as the longest PL decay lifetime of 2.74 ± 0.01 μs (Table 3 and Figure 7). Additional shell growth lowered the relative PL intensity, as observed previously for giant, thick-shelled CdSe/CdS core/shell nanocrystals (an effect that was attributed to the eventual appearance of cracks or defects due to increasingly large strain effects).[29,44,45] Nevertheless, all Ge/II–VI nanocrystals consistently showed one-to-three (10–1000×) orders of magnitude more intense NIR PL compared to the brightest bare Ge nanocrystals that we ever obtained, which produced only 0.0004% QY (if and when emission was detectable). In fact, Ge cores made by reduction of GeI_2 with nBuLi in

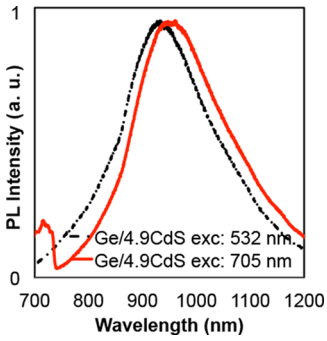

Figure 8. Photoluminescence spectra of Ge/4.9CdS nanocrystals collected with two different excitation wavelengths, λ_{exc} = 532 nm *vs* λ_{exc} = 705 nm (arbitrarily normalized).

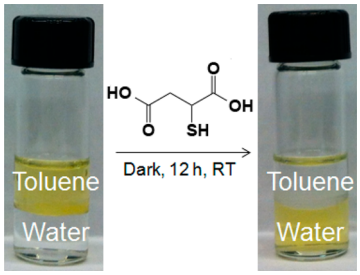

Scheme 2. Solubilization of Ge/4.9CdS nanocrystals in water *via* thiol ligand exchange.

hexadecylamine and ODE (see Methods) were only photo luminescent in a minority of cases; roughly one out of every 10 or 20 Ge batches made produced measurable PL. Because even the best Ge cores were very weakly emitting, we were unable to measure their PL lifetime (Figure 7b). While the lack of a Ge core-only excited-state lifetime prevents a definitive statement, we note that measured core/shell lifetimes, as shown in Figure 7 and summarized in Table 3 (single exponential fit of the long-lived decay), all fall within a factor of 5 of each other for various CdS shell thicknesses as well as for ZnS. Such comparable lifetimes suggest Type-I band alignment as suggested in Figure 2 for these compositions.

To confirm that Ge, rather than CdS traps, are responsible for the observed near-IR PL (900–1100 nm), we recollected the photoluminescence data utilizing a redder excitation. As shown in Figure 8, the PL spectra of Ge/CdS core/shell nanocrystals collected using 532 nm *vs* 705 nm laser excitation are very comparable. Because the CdS shell, with a band gap of *ca.* 520 nm (2.48 eV), cannot absorb or get excited with the much redder 705 nm laser, we conclude that the Ge core, rather than the CdS shell, is indeed responsible for the observed near-IR emission.

Aqueous Solubilization *via* Ligand Exchange. Ge/II–VI nanocrystals easily transfer from organic (typically toluene, hexane or chloroform) to aqueous phase upon ligand exchange with a suitable, water-soluble thiol. Scheme 2 graphically shows this procedure using Ge/4.9CdS and mercaptosuccinic acid as a representative example (see Methods) (Figure 9). Unfortunately,

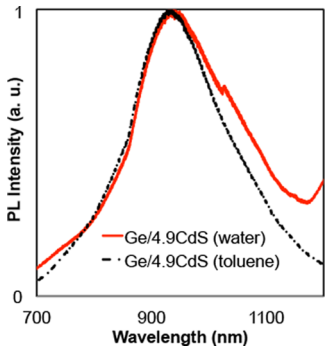

Figure 9. Photoluminescence spectra of Ge/4.9CdS core/shell nanocrystals in toluene and in water (after thiol ligand exchange) with $\lambda_{exc} = 532$ (the PL intensities are not relative and were arbitrarily normalized).

ligand exchange and/or water solubilization results in a decrease of PL intensity. However, the resulting water-soluble Ge/II−VI nanocrystals are still ten times (10×) brighter than the best, uncoated Ge cores (Table 3), which cannot be easily transferred to water.

CONCLUSIONS

Inspired by the prospect of using IV/II−VI epitaxy in colloidal semiconductors, we carried out a thorough investigation on the colloidal synthesis of thick-shelled Ge/MS (M = Cd or Zn) core/shell nanocrystals. We chose CdS and ZnS as shell materials based on their low lattice mismatch with crystalline Ge. Freshly prepared Ge cores were alternately reacted with enough metal (Cd or Zn) and sulfur (S) precursors to form one epitaxial atomic monolayer at a time using the SILAR method. Elemental mapping confirmed the presence and homogeneous distribution of Ge, M (Cd or Zn) and S elements in all samples. Further, we did not find any evidence of phase segregation in the several Ge/CdS and Ge/ZnS nanocrystals that we made and measured. In addition, analysis of Ge/CdS core/shells with different shell thickness showed a strong correlation between their theoretically expected and experimentally measured elemental compositions. We observed the shape evolution (morphology transformation) of Ge/CdS nanocrystals from spheres to tetrahedral prisms during shell growth. We believe the original cubic structure of the Ge cores played an important role in dictating the final morphology of the Ge/CdS core/shells. In contrast to Ge/CdS, Ge/ZnS nanocrystals did not show the expected larger particle size compared to the initial Ge cores. We tentatively attribute this behavior to combined etching and exchange effects of the specific Zn and/or S precursors used here on the original Ge nanocrystalline cores.

Growth of a II/VI (CdS or ZnS) shell greatly enhances the near-infrared (NIR) photoluminescence intensity and improves the NIR photoluminescence stability of Ge nanocrystals. In general, all Ge/II−VI heterostrucutures showed 1−3 orders of magnitude more intense NIR emission compared to the original Ge cores. All the Ge/II−VI nanocrystals retained their NIR photoluminescence after several months. Ge/4.9CdS showed the highest NIR quantum yield and longest PL lifetime. Although there is clearly room for improvement, the achieved PL level is already three thousand times brighter than the most emissive Ge cores we were able to make using literature procedures. Additional CdS shell growth caused a decrease in quantum yield, possibly because of the introduction of defects due to strain effects. Ge/II−VI nanocrystals easily transfer from organic to aqueous phase upon thiol ligand exchange. We expect that these results will extend the arsenal of quantum dot fluorophores available, particularly near-IR active quantum dots, for fundamental optoelectronic studies as well as for biological imaging and tracking, telecommunications, and energy conversion applications.

METHODS

Materials. Cadmium oxide (CdO, 99.998%), zinc oxide (ZnO, 99.99%), sulfur (S_8, 99.999%) and oleic acid (90%) were purchased from Alfa Aesar; *n*-butyllithium (*n*-BuLi, 1.6 M hexane solution), dioctylamine ($octyl_2NH$, 98%), tetramethylammoniumhydroxide pentahydrate ($Me_4NOH \cdot 5H_2O$, ≥97%) and mercaptosuccinic acid (97%) from Sigma-Aldrich; hexadecylamine ($hexadecylNH_2$, 98%) and 1-octadecene (ODE, 90%) from Acros; sodium chloride (NaCl) from Fisher; and germanium(II) iodide (GeI_2, 99.99+%-Ge) from Strem. Procedures were performed under a dry inert gas atmosphere (N_2 or Ar) inside a glovebox or a Schlenk line unless specified otherwise.

Synthesis. *Ge Cores.* Ge was synthesized by a modified literature procedure.[26] Inside a dry N_2-filled glovebox, GeI_2 (0.05 g, 0.15 mmol), hexadecylamine (0.75 g, 3.11 mmol) and a Teflon-coated stir bar were added to an oven dry, four-neck 250 mL round-bottom (RB) flask. The flask was fitted with a condenser, and the system was sealed and brought out and connected to a vacuum line. The contents were degassed under a vacuum at 80 °C for 30 min, refilled with dry Ar, and heated to 200 °C. After 5 min at this temperature, a mixture of *n*-BuLi (0.2 mL of 1.6 M hexane solution) and ODE (0.75 mL) made inside the dry-N_2 filled glovebox was quickly injected. The mixture was heated to and annealed at 300 °C for 1 h. The mixture was then allowed to cool down to rt. The freshly prepared Ge cores were allowed to remain in the crude solution (without washing) under a constant stream of dry Ar until further processing (see shell growth below).

Ge/MS Nanocrystals (M = Cd or Zn). Precursor solutions: Cd, Zn and S stock solutions were made by a previously reported procedure.[44] 0.2 M $Cd(oleate)_2$: CdO (318 mg, 2.48 mmol), oleic acid (3.09 g, 10.94 mmol), and ODE (7.11 g, 28.16 mmol) were degassed under a vacuum at 80 °C for 60 min, refilled with Ar, and heated to 240 °C until optically clear. 0.1 M $Cd(oleate)_2$-amine: $(octyl)_2NH$ (12.5 mL, 41.36 mmol) was degassed under a vacuum at 80 °C for 30 min, refilled with Ar, and transferred to another flask containing 0.2 M $Cd(oleate)_2$ (12.5 mL). The mixture was stirred at 60 °C for 20 min. 0.2 M $Zn(oleate)_2$: ZnO (203 mg, 2.49 mmol), oleic acid (6.18 g, 21.88 mmol), and ODE (4.41 g, 17.47 mmol) were degassed under a vacuum at 80 °C for 60 min, refilled with Ar, and heated to 240 °C until optically clear. 0.1 M $Zn(oleate)_2$-amine: $(octyl)_2NH$ (12.5 mL, 41.36 mmol) was degassed under a vacuum at 80 °C for 30 min, refilled with Ar,

and transferred to another flask containing 0.2 M Zn(oleate)$_2$ (12.5 mL). The mixture was stirred at 60 °C for 20 min. 0.1 M S_8 precursor solution: S_8 (79.0 mg, 2.47 mmol) and ODE (19.73 g, 78.13 mmol) were degassed under a vacuum at 80 °C for 30 min, refilled with Ar, heated to 180 °C for 20 min until optically clear. Shell growth: ODE (1.5 mL, 4.69 mmol) and dioctylamine (1.5 mL, 4.96 mmol) were introduced to the four-neck 250 mL RB flask containing freshly made Ge cores. The mixture was degassed under vacuum at 80 °C for 30 min, refilled with Ar, and heated to a constant shell growth temperature 230 °C. M (Cd or Zn) and S precursors were introduced in an alternating fashion using two programmable syringe pumps, each followed by a 15 min wait period. Either the S (preferred) precursor or the M precursor (Cd or Zn, also okay) was injected first. Shell growth was monitored by absorption or transmission electron microscopy (TEM) (below) using aliquots (0.05 mL) taken at different shell growth stages. The mixture was allowed to cool to rt 15 minutes after the last M (Cd or Zn) or S injection. Purification: Core/shell nanocrystals were washed three times by precipitation with 1:1 or 1:3 v/v acetone/methanol mixtures and centrifugation at 4200 rpm for 5 min, using each time toluene as the redissolution solvent. Transfer to water *via* ligand exchange: 0.5 mL of "crude" (unpurified) Ge/MS and mercaptosuccinic acid (100 mg, 0.67 mmol) were dissolved in toluene (2.5 mL). A solution of tetramethylammonium hydroxide pentahydrate (600 mg, 3.31 mmol) deionized water (3 mL) was added. The mixture was transferred into a vial coated with aluminum foil and vigorously stirred overnight. Water-soluble Ge/nMS were washed once or twice by precipitation with brine (saturated NaCl solution) and centrifugation at 4200 rpm for 5 min, using each time deionized water as redissolution solvent.

Structural Characterization. Powder X-ray diffraction (XRD) was measured using Cu Kα radiation on a Rigaku Ultima U4 diffractometer. Quantitative estimates of relative phase abundances (% cubic *versus* % hexagonal) of Ge/II−VI nanocrystals were performed using Rietveld analysis on PowderCell 2.3. Transmission electron microscopy (TEM) was conducted on carbon-coated copper grids using FEI Tecnai G2 F20 field emission scanning transmission electron microscope (STEM) at 200 kV (point-to-point resolution <0.25 nm, line-to-line resolution <0.10 nm). Elemental composition was characterized by energy-dispersive spectroscopy (EDS). For particle analysis, dimensions were measured manually or with ImageJ for >200 particles. Average sizes (diameters) are reported ± standard deviations.

Optical Characterization. Absorption spectra were measured with an Agilent 8453 UV−vis photodiode array spectrophotometer. Steady-state PL spectra were measured by exciting the sample with a 532 nm diode laser and directing the collected PL to a 0.3 m spectrometer and liquid nitrogen-cooled InGaAs photodiode array. Comparison of integrated PL intensity to the organic dye IR-26 (0.05% QY) was used to determine quantum yields (all measurements were collected at least twice).[65,66] Time-resolved PL was measured using time-correlated single photon counting (TCSPC). Samples were photoexcited with a 35 ps pulsewidth, 450 nm diode laser operated between 100 and 400 kHz. TCSPC was then recorded at the PL spectrum maximum using an avalanche photodiode.

Conflict of Interest: The authors declare no competing financial interest.

Acknowledgment. J. Vela gratefully acknowledges the National Science Foundation for funding of this work through a CAREER grant from the Division of Chemistry, Macromolecular, Supramolecular and Nanochemistry (MSN) program (NSF-CHE-1253058). This work was performed, in part, at the Center for Nanoscale Materials, a U.S. Department of Energy, Office of Science, Office of Basic Energy Sciences User Facility under Contract No. DE-AC02-06CH11357. Y. Guo is the recipient of an Iowa State University Research Excellence Award and a scholarship from the Midwest Chapter of the Society of Cosmetic Chemists. C. Rowland acknowledges support from a National Science Foundation Graduate Research Fellowship (NSF-DGE-0824162). J. Vela and Y. Guo thank Iowa State University's Plant Sciences Institute for initial support, as well as Purnima Ruberu and Sam Alvarado for assistance with synthesis and graphics.

Supporting Information Available: TEM and particle size data for Ge/ZnS nanocrystals. This material is available free of charge *via* the Internet at http://pubs.acs.org.

REFERENCES AND NOTES

1. Vaughn, D. D., II; Schaak, R. E. Synthesis, Properties and Applications of Colloidal Germanium and Germanium-Based Nanomaterials. *Chem. Soc. Rev.* **2013**, *42*, 2861–2879.
2. Cullis, A. G.; Canham, L. T.; Calcott, P. D. J. The Structural and Luminescence Properties of Porous Silicon. *Appl. Phys. Rev.* **1997**, *82*, 909–965.
3. Maeda, Y.; Tsukamoto, N.; Yazawa, Y.; Kanemitsu, Y.; Masumoto, Y. Visible Photoluminescence of Ge Microcrystals Embedded in SiO_2 Glassy Matrices. *Appl. Phys. Lett.* **1991**, *59*, 3168–3170.
4. Wu, Y.; Yang, P. Germanium Nanowire Growth *via* Simple Vapor Transport. *Chem. Mater.* **2000**, *12*, 605–607.
5. Sánchez-Pérez, J. R.; Boztug, C.; Chena, F.; Sudradjat, F. F.; Paskiewicz, D. M.; Jacobson, R. B.; Lagally, M. G.; Paiella, R. Direct-Bandgap Light-Emitting Germanium in Tensilely Strained Nanomembranes. *Proc. Natl. Acad. Sci. U. S. A.* **2011**, *108*, 18893–18898.
6. Sun, X.; Liu, J.; Kimerling, L. C.; Michel, J. Direct Gap Photoluminescence of n-Type Tensile-Strained Ge-on-Si. *Appl. Phys. Lett.* **2009**, *95*, 011911−1–011911−3.
7. Pavarelli, N.; Ochalski, T. J.; Murphy-Armando, F.; Huo, Y.; Schmidt, M.; Huyet, G.; Harris, J. S. Optical Emission of a Strained Direct-Band-Gap Ge Quantum Well Embedded Inside InGaAs Alloy Layers. *Phys. Rev. Lett.* **2013**, *110*, 177404−1–177404−5.
8. Camacho-Aguilera, R.; Han, Z.; Cai, Y.; Kimerling, L. C.; Michel, J. Direct Band Gap Narrowing in Highly Doped Ge. *Appl. Phys. Lett.* **2013**, *102*, 152106−1–152106−3.
9. Lu, X. M.; Korgel, B. A.; Johnston, K. P. High Yield of Germanium Nanocrystals Synthesized from Germanium Diiodide in Solution. *Chem. Mater.* **2005**, *17*, 6479–6485.
10. Vaughn, D. D., II; Bondi, J. F.; Schaak, R. E. Colloidal Synthesis of Air-Stable Crystalline Germanium Nanoparticles with Tunable Sizes and Shapes. *Chem. Mater.* **2010**, *22*, 6103–6108.
11. Muthuswamy, E.; Iskandar, A. S.; Amador, M. M.; Kauzlarich, S. M. Facile Synthesis of Germanium Nanoparticles with Size Control: Microwave *versus* Conventional Heating. *Chem. Mater.* **2013**, *25*, 1416–1422.
12. Dag, Ö; Henderson, E. J.; Ozin, G. A. Synthesis of Nanoamorphous Germanium and Its Transformation to Nanocrystalline Germanium. *Small* **2012**, *8*, 921–929.
13. Henderson, E. J.; Hessel, C. M.; Cavell, R. G.; Veinot, J. G. C. How Processing Atmosphere Influences the Evolution of GeO_2-Embedded Germanium Nanocrystals Obtained from the Thermolysis of Phenyl Trichlorogermane-Derived Polymers. *Chem. Mater.* **2010**, *22*, 2653–2661.
14. Hoffman, M.; Veinot, J. G. C. Understanding the Formation of Elemental Germanium by Thermolysis of Sol-Gel Derived Organogermanium Oxide Polymers. *Chem. Mater.* **2012**, *24*, 1283–1291.
15. Kim, C. H.; Im, H. S.; Cho, Y. J.; Jung, C. S.; Jang, D. M.; Myung, Y.; Kim, H. S.; Back, S. H.; Lim, Y. R.; Lee, C.-W.; *et al.* High-Yield Gas-Phase Laser Photolysis Synthesis of Germanium Nanocrystals for High-Performance Photodetectors and Lithium Ion Batteries. *J. Phys. Chem. C* **2012**, *116*, 26190–26196.
16. Henderson, E. J.; Veinot, J. G. C. Synthesis of Oxide Encapsulated and Freestanding Hydride Surface Terminated $Si_{1-x}Ge_x$ Nanocrystals. *Chem. Mater.* **2007**, *19*, 1886–1888.
17. Ruddy, D. A.; Erslev, P. T.; Habas, S. E.; Seabold, J. A.; Neale, N. R. Surface Chemistry Exchange of Alloyed Germanium Nanocrystals: A Pathway Toward Conductive Group IV Nanocrystal Films. *J. Phys. Chem. Lett.* **2013**, *4*, 416–421.
18. Chou, N. H.; Oyler, K. D.; Motl, N. E.; Schaak, R. E. Colloidal Synthesis of Germanium Nanocrystals Using Room-Temperature Benchtop Chemistry. *Chem. Mater.* **2009**, *21*, 4105–4107.

19. Shirahata, N.; Hirakawa, D.; Masuda, Y.; Sakka, Y. Size-Dependent Color Tuning of Efficiently Luminescent Germanium Nanoparticles. *Langmuir* **2013**, *29*, 7401–7410.
20. Armatas, G. S.; Kanatzidis, M. G. Size Dependence in Hexagonal Mesoporous Germanium: Pore Wall Thickness *versus* Energy Gap and Photoluminescence. *Nano Lett.* **2010**, *10*, 3330–3336.
21. Armatas, G. S.; Kanatzidis, M. G. Mesoporous Compound Semiconductors from the Reaction of Metal Ions with Deltahedral $[Ge_9]^{4-}$ Clusters. *J. Am. Chem. Soc.* **2008**, *130*, 11430–11436.
22. Bag, S.; Trikalitis, P. N.; Chupas, P. J.; Armatas, G. S.; Kanatzidis, M. G. Porous Semiconducting Gels and Aerogels from Chalcogenide Clusters. *Science* **2007**, *317*, 490–493.
23. Armatas, G. S.; Kanatzidis, M. G. Mesoporous Germanium-Rich Chalcogenido Frameworks with Highly Polarizable Surfaces and Relevance to Gas Separation. *Nat. Mater.* **2009**, *8*, 217–222.
24. Kanatzidis, M. G. Beyond Silica: Nonoxidic Mesostructured Materials. *Adv. Mater.* **2007**, *19*, 1165–1181.
25. Armatas, G. S.; Kanatzidis, M. G. High-Surface-Area Mesoporous Germanium from Oxidative Polymerization of the Deltahedral $[Ge_9]^{4-}$ Cluster: Electronic Structure Modulation with Donor and Acceptor Molecules. *Adv. Mater.* **2008**, *20*, 546–550.
26. Lee, D. C.; Pietryga, J. M.; Robel, I.; Werder, D. J.; Schaller, R. D.; Klimov, V. I. Colloidal Synthesis of Infrared-Emitting Germanium Nanocrystals. *J. Am. Chem. Soc.* **2009**, *131*, 3436–3437.
27. Ruddy, D. A.; Johnson, J. C.; Smith, E. R.; Neale, N. R. Size and Bandgap Control in the Solution-Phase Synthesis of Near-Infrared-Emitting Germanium Nanocrystals. *ACS Nano* **2010**, *4*, 7459–7466.
28. Wheeler, L. M.; Levij, L. M.; Kortshagen, U. R. Tunable Band Gap Emission and Surface Passivation of Germanium Nanocrystals Synthesized in the Gas Phase. *J. Phys. Chem. Lett.* **2013**, *4*, 3392–3396.
29. Chen, Y.; Vela, J.; Htoon, H.; Casson, J. L.; Werder, D. J.; Bussian, D. A.; Klimov, V. I.; Hollingsworth, J. A. "Giant" Multishell CdSe Nanocrystal Quantum Dots with Suppressed Blinking. *J. Am. Chem. Soc.* **2008**, *130*, 5026–5027.
30. Mahler, B.; Spinicelli, P.; Buil, S.; Quelin, X.; Hermier, J. P.; Dubertret, B. Towards Non-Blinking Colloidal Quantum Dots. *Nat. Mater.* **2008**, *7*, 659–664.
31. Dennis, A. M.; Mangum, B. D.; Piryatinski, A.; Park, Y.-S.; Hannah, D. C.; Casson, J. L.; Williams, D. J.; Schaller, R. D.; Htoon, H.; Hollingsworth, J. A. Suppressed Blinking and Auger Recombination in Near-Infrared Type-II InP/CdS Nanocrystal Quantum Dots. *Nano Lett.* **2012**, *12*, 5545–5551.
32. Lee, D. C.; Robel, I.; Jeffrey M. Pietryga, J. M.; Klimov, V. I. Infrared-Active Heterostructured Nanocrystals with Ultralong Carrier Lifetimes. *J. Am. Chem. Soc.* **2010**, *132*, 9960–9962.
33. Pietryga, J. M.; Werder, D. J.; Williams, D. J.; Casson, J. L.; Schaller, R. D.; Klimov, V. I.; Hollingsworth, J. A. Utilizing the Lability of Lead Selenide to Produce Heterostructured Nanocrystals with Bright, Stable Infrared Emission. *J. Am. Chem. Soc.* **2008**, *130*, 4879–4885.
34. Pietryga, J. M.; Schaller, R. D.; Werder, D.; Stewart, M. H.; Klimov, V. I.; Hollingsworth, J. A. Pushing the Band Gap Envelope: Mid-Infrared Emitting Colloidal PbSe Quantum Dots. *J. Am. Chem. Soc.* **2004**, *126*, 11752–11753.
35. Pichaandi, J.; van Veggel, F. C. J. M. Near-Infrared Emitting Quantum Dots: Recent Progress on Their Synthesis and Characterization. *Coord. Chem. Rev.* **2014**, *263–264*, 138–150.
36. Van Veggel, F. C. J. M. Near-Infrared Quantum Dots and Their Delicate Synthesis, Challenging Characterization, and Exciting Potential Applications. *Chem. Mater.* **2014**, *26*, 111–122.
37. Reiss, P.; Protière, M.; Li, L. Core/Shell Semiconductor Nanocrystals. *Small* **2009**, *5*, 154–168.
38. Rogach, A. L.; Eychmuüller, A.; Hickey, S. G.; Kershaw, S. V. Infrared-Emitting Colloidal Nanocrystals: Synthesis, Assembly, Spectroscopy, and Applications. *Small* **2007**, *3*, 536–557.
39. Gejji, F. H.; Holt, D. B. Epitaxial Growth and Structure of CdSe Evaporated in Vacuum onto Ge. *J. Electrochem. Soc.* **1975**, *122*, 535–541.
40. Paorici, C. G. C.; Pelosi, C.; Servidori, M. Growth and Defect Strucuture of CdS Epitaxial Layers on (111) Ge Substrates. *J. Cryst. Growth* **1977**, *41*, 181–191.
41. Zhang, J.; Tang, Y.; Lee, K.; Ouyang, M. Nonepitaxial Growth of Hybrid Core-Shell Nanostructures with Large Lattice Mismatches. *Science* **2010**, *327*, 1634–1638.
42. Lambright, S.; Butaeva, E.; Razgoniaeva, N.; Hopkins, T.; Smith, B.; Perera, D.; Corbin, J.; Khon, E.; Thomas, R.; Moroz, P.; *et al.* Enhanced Lifetime of Excitons in Nonepitaxial Au/CdS Core/Shell Nanocrystals. *ACS Nano* **2014**, *8*, 352–361.
43. Embden, J. V.; Jasieniak, J.; Mulvaney, P. Mapping the Optical Properties of CdSe/CdS Heterostructure Nanocrystals: The Effects of Core Size and Shell Thickness. *J. Am. Chem. Soc.* **2009**, *131*, 14299–14309.
44. Vela, J.; Htoon, H.; Chen, Y.; Park, Y.-S.; Ghosh, Y.; Goodwin, P.; Werner, J.; Wells, N. P.; Casson, J. L.; Hollingsworth, J. A. Effect of Shell Thickness and Composition on Blinking Suppression and the Blinking Mechanism in Giant CdSe/CdS Nanocrystal Quantum Dots. *J. Biophoton.* **2010**, *3*, 706–717.
45. Guo, Y.; Marchuk, K.; Sampat, S.; Abraham, R.; Fang, N.; Malko, A.; Vela, J. Unique Challenges Accompany Thick-Shell CdSe/*n*CdS ($n > 10$) Nanocrystal Synthesis. *J. Phys. Chem. C* **2012**, *116*, 2791–2800.
46. Efros, A. L. Nanocrystals Almost Always Bright. *Nat. Mater.* **2008**, *7*, 612–613.
47. Piryatinski, A.; Ivanov, S. A.; Tretiak, S.; Klimov, V. I. Effect of Quantum and Dielectric Confinement on the Exciton–Exciton Interaction Energy in Type II Core/Shell Semiconductor Nanocrystals. *Nano Lett.* **2007**, *7*, 108–115.
48. García-Santamaría, F.; Chen, Y.; Vela, J.; Schaller, R. D.; Hollingsworth, J. A.; Klimov, V. I. Suppressed Auger Recombination in "Giant" Nanocrystals Boosts Optical Gain Performance. *Nano Lett.* **2009**, *9*, 3482–3488.
49. Mahler, B.; Lequeux, N.; Dubertret, B. Ligand-Controlled Polytypism of Thick-Shell CdSe/CdS Nanocrystals. *J. Am. Chem. Soc.* **2010**, *132*, 953–959.
50. Tschirner, N.; Lange, H.; Schliwa, A.; Biermann, A.; Thomsen, C.; Lambert, K.; Gomes, R.; Hens, Z. Interfacial Alloying in CdSe/CdS Heteronanocrystals: A Raman Spectroscopy Analysis. *Chem. Mater.* **2012**, *24*, 311–317.
51. Dzhagan, V. M.; Valakh, M. Y.; Raevska, O. E.; Stroyuk, O. L.; Kuchmiy, S. Y.; Zahn, D. R. T. The Influence of Shell Parameters on Phonons in Core-Shell Nanoparticles: A Resonant Raman Study. *Nanotechnology* **2009**, *20*, 365704–1–365704–6.
52. Dzhagan, V. M.; Valakh, M. Y.; Milekhin, A. G.; Yeryukov, N. A.; Zahn, D. R. T.; Cassette, E.; Pons, T.; Dubertret, B. Raman- and IR-Active Phonons in CdSe/CdS Core/Shell Nanocrystals in the Presence of Interface Alloying and Strain. *J. Phys. Chem. C* **2013**, *117*, 18225–18233.
53. Vela, J. Molecular Chemistry to the Fore: New Insights into the Fascinating World of Photoactive Colloidal Semiconductor Nanocrystals. *J. Phys. Chem. Lett.* **2013**, *4*, 653–668.
54. Marchuk, K.; Guo, Y.; Sun, W.; Vela, J.; Fang, N. High-Precision Tracking with Non-blinking Quantum Dots Resolves Nanoscale Vertical Displacement. *J. Am. Chem. Soc.* **2012**, *134*, 6108–6111.
55. Lesoine, M. D.; Bhattacharjee, U.; Guo, Y.; Vela, J.; Petrich, J. W.; Smith, E. A. Subdiffraction, Luminescence-Depletion Imaging of Isolated, Giant, CdSe/CdS Nanocrystal Quantum Dots. *J. Phys. Chem. C* **2013**, *117*, 3662–3667.
56. McBride, J.; Treadway, J.; Feldman, L. C.; Pennycook, S. J.; Rosenthal, S. J. Structural Basis for Near Unity Quantum Yield Core/Shell Nanostructures. *Nano Lett.* **2006**, *6*, 1496–1501.
57. Li, J. J.; Wang, Y. A.; Guo, W. Z.; Keay, J. C.; Mishima, T. D.; Johnson, M. B.; Peng, X. G. Large-scale Synthesis of Nearly Monodisperse CdSe/CdS Core/Shell Nanocrystals Using Air-Stable Reagents *via* Successive Ion Layer Adsorption and Reaction. *J. Am. Chem. Soc.* **2003**, *125*, 12567–12575.

58. Son, D. H.; Hughes, S. M.; Yin, Y.; Alivisatos, A. P. Cation Exchange Reactions in Ionic Nanocrystals. *Science* **2004**, *306*, 1009–1012.
59. Beberwyck, B. J.; Surendranath, Y.; Alivisatos, A. P. Cation Exchange: A Versatile Tool for Nanomaterials Synthesis. *J. Phys. Chem. C* **2013**, *117*, 19759–19770.
60. Rivest, J. B.; Jain, P. K. Cation Exchange on the Nanoscale: An Emerging Technique for New Material Synthesis, Device Fabrication, and Chemical Sensing. *Chem. Soc. Rev.* **2013**, *42*, 89–96.
61. Gupta, S.; Kershaw, S. V.; Rogach, A. L. 25th Anniversary Article: Ion Exchange in Colloidal Nanocrystals. *Adv. Mater.* **2013**, *25*, 6923–6944.
62. Wang, X.; Ren, X.; Kahen, K.; Hahn, M. A.; Rajeswaran, M.; Sara Maccagnano-Zacher, S.; Silcox, J.; Cragg, G. E.; Efros, A. L.; Krauss, T. D. Non-Blinking Semiconductor Nanocrystals. *Nature* **2009**, *459*, 686–689.
63. Pearson, R. G. Hard and Soft Acids and Bases. *J. Am. Chem. Soc.* **1963**, *85*, 3533–3534.
64. Pearson, R. G. Hard and Soft Acids and Bases—The Evolution of a Chemical Concept. *Coord. Chem. Rev.* **1990**, *100*, 403–425.
65. Benfey, D. P.; Brown, D. C.; Davis, S. J.; Piper, L. G.; Foutter, R. F. Diode-Pumped Dye Laser Analysis and Design. *Appl. Opt.* **1992**, *31*, 7034–7041.
66. Semonin, O. E.; Johnson, J. C.; Luther, J. M.; Midgett, A. G.; Nozik, A. J.; Beard, M. C. Absolute Photoluminescence Quantum Yields of IR-26 Dye, PbS, and PbSe Quantum Dots. *J. Phys. Chem. Lett.* **2010**, *1*, 2445–2450.